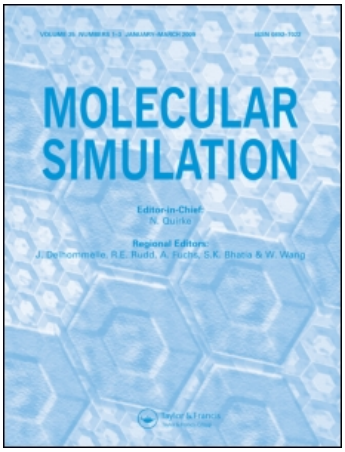

Molecular Simulation
Publication details, including instructions for authors and subscription information:
http://www.informaworld.com/smpp/title~content=t713644482

Modelling the viscoelasticity and thermal fluctuations of fluids at the nanoscale

Nikolaos K. Voulgarakis[a]; Siddarth Satish[a]; Jhih-Wei Chu[a]
[a] Department of Chemical Engineering, University of California, Berkeley, CA, USA

Online publication date: 03 August 2010

To cite this Article Voulgarakis, Nikolaos K. , Satish, Siddarth and Chu, Jhih-Wei(2010) 'Modelling the viscoelasticity and thermal fluctuations of fluids at the nanoscale', Molecular Simulation, 36: 7, 552 — 559
To link to this Article: DOI: 10.1080/08927022.2010.486832
URL: http://dx.doi.org/10.1080/08927022.2010.486832

Molecular Simulation
Vol. 36, Nos. 7–8, June–July 2010, 552–559

Taylor & Francis
Taylor & Francis Group

Modelling the viscoelasticity and thermal fluctuations of fluids at the nanoscale

Nikolaos K. Voulgarakis[†], Siddarth Satish[†] and Jhih-Wei Chu*

Department of Chemical Engineering, University of California, Berkeley, CA, USA

(*Received 8 February 2010; final version received 9 April 2010*)

Simulation methodologies for modelling the viscoelasticity and thermal fluctuations of molecular fluids at nanoscale are presented. In particular, we bridge the distinct frameworks of fluctuating hydrodynamics (FHD) and molecular dynamics (MD) simulations using a coarse-graining procedure that properly considers the effective size of each fluid molecule in mapping a phase space vector of the all-atom model to field variables in the FHD representation. We also generalise the FHD equations to model non-Markovian rheological responses by incorporating coloured noise. To capture the increasing elastic responses that emerge at the nanoscale, a composite Newtonian–Maxwell rheological model is developed. Numerical simulations using a staggered discretisation scheme demonstrate that the thermodynamic states and dynamic properties (power spectra) of FHD equations match with those of all-atom MD simulations quantitatively. This agreement also unambiguously determines the wavenumber-dependent transport coefficients of the composite Newtonian–Maxwell model. To avoid the complexities associated with using wavenumber-dependent transport coefficients, we characterise the approximation of using a single set of transport coefficients. We find that for collective fluctuations with a wavelength longer than 25 Å, wavenumber-independent models can accurately describe the power spectra. For fluctuations with shorter wavelengths, relative errors in power spectra increase monotonically with wavenumber.

Keywords: fluctuating hydrodynamics; viscoelasticity; nanoscale; coarse grain; molecular dynamics

1. Introduction

Hydrodynamic interactions and thermal fluctuations are the essential driving forces of dynamic processes at the nanoscale. Characterising the rheological properties of fluids in the presence of density and momentum fluctuations is thus relevant to a wide range of topics, including intra- and inter-cellular fluid dynamics and nano-fluidics [1–5]. While atomic scale simulations provide an accurate representation of molecular dynamics (MD), the limited time- and length-scales prevent an effective modelling of the collective hydrodynamic interactions between nanosized objects [6,7]. Accurate and robust computational methods for describing hydrodynamic interactions in the mesoscopic regime are thus in urgent need. For this purpose, the equations of fluctuating hydrodynamics (FHD) proposed by Landau and Lifshitz [8] provide a fundamental framework based on which many simulation methods such as smooth particle hydrodynamics [9], Lattice Boltzmann [10], and dissipative particle dynamics [11,12], are developed. A strategy that is often employed is to transform the field representation of governing equations into a Lagrangian form by defining effective particles and determining the interactions between them [9,11,12]. One motivation for transforming the FHD equations into a particle-based representation is to build in the flexibility of modelling complex geometries and multiphase flows. However, particle-based representations only approximately satisfy the FHD equations. Density fluctuations are also not fully captured since the exchange of mass between effective fluid particles is not considered. These discrepancies to FHD equations often make the interpretation of simulation results difficult.

On the other hand, directly solving the FHD equations on numerical grids [13–18] also encounters difficulties such as numerical instability when using small grid sizes (<1 nm), the need for modelling density fluctuations instead of assuming incompressibility, the requirement of describing thermodynamic states by balancing dissipative and fluctuating forces with high accuracy and achieving consistency between FHD and MD simulations. An increasing amount of effort is thus being devoted to develop accurate and stable numerical solvers for FHD equations [13–18]. In this regard, we have recently developed a staggered discretisation scheme [18] that uses distinct grid points to represent density and momentum variables separately. The staggered scheme significantly enhances the accuracy of numerical solutions compared to non-staggered schemes [17], especially when small cell sizes and large density fluctuations are involved [18].

*Corresponding author. Email: jwchu@berkeley.edu
[†]Both authors contributed equally to this work.

ISSN 0892-7022 print/ISSN 1029-0435 online

DOI: 10.1080/08927022.2010.486832
http://www.informaworld.com

For modelling transient flows, the staggered discretisation scheme can capture the causative relationship between field variables and hence prevent the occurrence of unphysical relaxation processes [18].

In establishing consistency between all-atom MD and FHD simulations, we developed a mapping from the position and velocity vectors of atoms in a molecular model to hydrodynamic field variables by utilising the Irving and Kirkwood [19] procedure and demonstrated that the thermodynamic states of FHD and MD models as measured by the fluctuations of field variables can be matched quantitatively [18]. A key element of this mapping is the effective size of molecules, d_{mol}, used to calculate the fractional contributions of each molecule to the density of a grid cell. We show that the values of d_{mol} can be determined via the excluded molecular radii as observed in the radial distribution functions of molecular fluids [18].

Another important aspect of hydrodynamics at the nanoscale is the complex stress responses due to a combination of dynamic processes that occur at different length scales and timescales. For example, non-Markovian responses such as elasticity can emerge at small length scales [20–23]. To address these issues, we generalised the FHD framework to include viscoelastic constitutive equations [24]. In particular, we developed a rheological model by attaching a linear Maxwell model [25] in parallel to the macroscopic constitutive equation of a Newtonian fluid to characterise the viscous and elastic behaviours that emerge at the nanoscale. We used the approach of generalised Langevin equation to model the time evolution with coloured noise [24]. This model is validated by matching the power spectra obtained from all-atom MD simulations with the results of Normal Mode Analysis on linearised FHD equations [24]. The results indicate that the composite rheological model provides an accurate representation of the wavenumber (q)-dependent transport coefficients of molecular fluids at the nanoscale [24]. Despite the success of generalising FHD equations to model viscoelasticity, an important question that we aim to address in this work is whether the q-independent transport coefficients can be modelled with a single set of representative parameters instead of keeping track of the whole spectra. This approach would greatly reduce the complexity of modelling the viscoelasticity of fluids at the nanoscale.

In the following, we first briefly review the theoretical and numerical framework that we developed for solving the FHD equations. We then perform a least-squares fit using a single set of transport coefficients of the composite viscoelastic model to the full power spectra calculated from all-atom MD simulations of liquid argon and water. Our results indicate that using a single set of transport coefficients describe well the hydrodynamic responses with a wavelength longer than 25 Å.

2. Methods

2.1 The equations of FHD and a composite Newtonian–Maxwell model

We generalise the FHD equations of Landau and Lifshitz [8] to describe the conservation of mass and momentum of a compressible fluid in the presence of thermally induced fluctuations:

$$\begin{aligned}\frac{\partial \rho}{\partial t} &= -\,\partial_\alpha g_\alpha \\ \frac{\partial r_\alpha}{\partial t} &= -\,\frac{1}{\tau} r_\alpha + \frac{1}{\rho} g_\alpha \\ \frac{\partial g_\alpha}{\partial t} &= -\,\partial_\beta P - \partial_\beta (g_\beta u_\alpha + T^{\alpha\beta} + T_{el}^{\alpha\beta} + \tilde{T}^{\alpha\beta} + \tilde{T}_{el}^{\alpha\beta}).\end{aligned} \tag{1}$$

In Equation (1), a vector field r_α is introduced to calculate the effective displacements from momentum fields with a phenomenological relaxation time, τ, to model the elastic responses of a fluid at the nanoscale. Other variables in Equation (1) are defined as follows: ρ is mass density, g_α is the momentum field along one of the three Cartesian directions, i.e. α, $\beta = x$, y or z and Einstein's notation is employed and $u_\alpha = g_\alpha/\rho$ is the velocity field. Hydrostatic pressure is calculated from the density field through the following equation of state, although any other equation of state can be employed,

$$P = c_T^2 \rho, \tag{2}$$

where c_T is the isothermal sound velocity. For a macroscopically Newtonian fluid, the $\alpha\beta$ component of the stress tensor, $T^{\alpha\beta}$, is:

$$\begin{aligned}T^{\alpha\beta} = &-\eta\left(\partial_\alpha u_\beta + \partial_\beta u_\alpha - \frac{2}{3}\partial_\gamma u_\gamma \delta_{\alpha\beta}\right) \\ &- \eta_{\mathrm{B}} \partial_\gamma u_\gamma \delta_{\alpha\beta},\end{aligned} \tag{3}$$

where η and η_{B} represent the shear and bulk viscosity, respectively, and $\delta_{\alpha\beta}$ is the Kronecker delta.

The vector field r_α in Equation (1) represents the effective displacements with the following expression:

$$r_\alpha(t) = \int_0^t K(t - t') g_\alpha(t')\, \mathrm{d}t'. \tag{4}$$

In Equation (4), $K(t) = \mathrm{e}^{-t/\tau}/\rho$ is the memory kernel for calculating r_α from momentum fields. The values of r_α are then used to compute the elastic strain tensor, $T_{el}^{\alpha\beta}$. The $\alpha\beta$ component of $T_{el}^{\alpha\beta}$ is described via a linear model:

$$\begin{aligned}T_{el}^{\alpha\beta} = &-\kappa\left(\partial_\alpha r_\beta + \partial_\beta r_\alpha - \frac{2}{3}\partial_\gamma r_\gamma \delta_{\alpha\beta}\right) \\ &- \kappa_{\mathrm{B}} \partial_\gamma r_\gamma \delta_{\alpha\beta},\end{aligned} \tag{5}$$

where κ and κ_B are shear and bulk elastic modulus, respectively. The equations of r_α and $T_{el}^{\alpha\beta}$ correspond to the commonly used Maxwell model [25] for describing the rheological behaviours of viscoelastic fluids. The total stress in Equation (1) is the sum of two terms, $T^{\alpha\beta}$ and $T_{el}^{\alpha\beta}$, where $T^{\alpha\beta}$ comes from a reference macroscopic model (for which we assume that the fluid is Newtonian). The addition of $T_{el}^{\alpha\beta}$ in parallel to $T^{\alpha\beta}$ aims to capture the emergent elastic responses at the nanoscale. This treatment results in a composite Newtonian–Maxwell model and its power spectrum will be compared with those calculated from all-atom MD simulations for validation.

2.2 Numerical solutions of the FHD equations

At the nanoscale, thermal fluctuations are important driving forces for transport processes [1–5]; a fluctuating component of the stress tensor is thus added to the momentum equations [8,17,18,24]. Fluctuating stresses of the rheological model described in Equation (1) are represented as $\tilde{T}^{\alpha\beta}$ and $\tilde{T}_{el}^{\alpha\beta}$; their dissipative counterparts are $T^{\alpha\beta}$ and $T_{el}^{\alpha\beta}$, respectively. Analogous to $T^{\alpha\beta}$ (Equation (3)), $\tilde{T}^{\alpha\beta}$ also includes contributions from shear ($\tilde{T}_S^{\alpha\beta}$) and bulk ($\tilde{T}_B$) parts, i.e. $\tilde{T}^{\alpha\beta} = \tilde{T}_S^{\alpha\beta} + \tilde{T}_B\delta_{\alpha\beta}$. The shear and bulk components of the fluctuating stress tensor, $\tilde{T}_S^{\alpha\beta}$ and $\tilde{T}_B$, can be evaluated through the fluctuation–dissipation theorem [17]:

$$\tilde{T}_S^{\alpha\beta} = \sqrt{\frac{4\eta k_B T}{\mathrm{d}tV}}\bar{W}^{\alpha\beta}, \quad \tilde{T}_B = \sqrt{\frac{2\eta_B k_B T}{3\mathrm{d}tV}}Tr[W], \qquad (6)$$

where k_B is the Boltzmann constant, T is the temperature, V is the volume of a fluid cell, dt is the integration time step and $W^{\alpha\beta}$ are Gaussian white noises with a variance of 1 that satisfy:

$$\langle W^{\alpha\beta}(\mathbf{r})W^{\gamma\delta}(\mathbf{r}')\rangle = \delta_{\alpha\gamma}\delta_{\beta\delta}\delta(\mathbf{r}-\mathbf{r}')$$
$$\bar{W} = \frac{W+W^T}{2} - \frac{Tr[W]}{3}\mathbf{1}. \qquad (7)$$

To employ the composite Newtonian–Maxwell model proposed earlier with thermal fluctuations, it is required to model the fluctuating stress tensor with coloured noise. Following the approach of solving the generalised Langevin equations [26,27], $\tilde{T}_{el}^{\alpha\beta}$ is calculated as

$$\frac{\partial\tilde{T}_{S,el}^{\alpha\beta}}{\partial t} = -\frac{\tilde{T}_{S,el}^{\alpha\beta}}{\tau} + \sqrt{\frac{4\kappa k_B T}{\tau\mathrm{d}tV}}\bar{W}^{\alpha\beta},$$
$$\frac{\partial\tilde{T}_{B,el}}{\partial t} = -\frac{\tilde{T}_{B,el}}{\tau} + \sqrt{\frac{2\kappa_B k_B T}{\tau\mathrm{d}tV}}Tr[W]. \qquad (8)$$

Similar to the fluctuating components of the viscous stress tensor, $\tilde{T}_{S,el}^{\alpha\beta}$ and $\tilde{T}_{B,el}$ comprise the shear and bulk parts of $\tilde{T}_{el}^{\alpha\beta}$, respectively ($\tilde{T}_{el}^{\alpha\beta} = \tilde{T}_{S,el}^{\alpha\beta} + \tilde{T}_{B,el}\delta_{\alpha\beta}$).

The non-Markovian FHD equations with coloured noise are solved using the staggered spatial discretisation scheme that we previously developed [18]. The motivation for employing a staggered algorithm is to capture the causality between density and momentum fluxes in the governing equations, and this approach can avoid unphysical phenomena when simulating transient flows [18]. We consider a fluid in a cubic box with a side length of a, and use N equally sized grids along each direction for spatial discretisation. The length of each side of a cell, d, is thus a/N. The arrangement of grid points projected on to the $x-y$ plane of a molecular simulation is shown in Figure 1. In the staggered discretisation scheme we developed, grid points of density fields are located at cell centres, and grid points of momentum fields are located at cell faces. The hydrodynamic equations are approximated in a discrete form following the central-difference method [18]. The net inward mass flux to a cell is calculated from the six momentum fields associated with its faces, and the velocity fields for grids at cell centres are calculated from the averaged momentum field of neighbouring grids at cell faces divided by the density field [18]. The velocity fields of grids at cell faces, on the other hand, are calculated via dividing the corresponding momentum field by the averaged mass density of the two adjacent grids at the cell centres. Depending on the constitutive equation, both diagonal and off-diagonal terms of the stress tensor components can be calculated by the velocity or displacement fields of nearby grids at cell faces. A variety of temporal discretisation schemes can be applied to solve

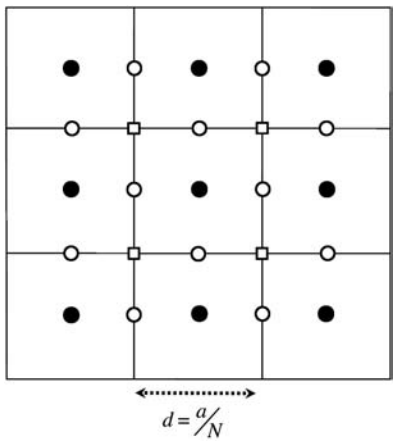

Figure 1. A schematic representation in 2D of the staggered discretisation scheme we developed for solving the FHD equations. Filled circles correspond to the grid points of mass density, diagonal terms of the stress tensor and hydrodynamic pressure. Open circles correspond to the grids of momentum fields at cell faces. Open squares correspond to the grids of the off-diagonal elements of the stress tensor. The filled circle at the centre of each cell is assigned with an index vector n (see Ref. [18] for details).

the FHD equations numerically, and we employed a second-order Runge–Kutta method [18,24].

The results [18,24] of numerical simulations illustrate that the staggered discretisation scheme not only prevented unphysical propagation of density fields in modelling a transient flow [18] but also gives a very high accuracy in describing the temperature of fluctuating fields. High stability and accuracy are achieved for both viscous and viscoelastic constitutive equations.

2.3 *Bridging FHD and all-atom MD simulations*

We developed a mapping to determine field variables from a phase space vector of the all-atom model to ensure that the thermodynamic states of MD and FHD simulations are consistent [18]. As shown in Figure 2, the domain of MD simulation is spatially discretised into cubic cells over which FHD equations are solved. Although the standard Irving and Kirkwood [19] procedure can be applied, we found that explicit consideration of the finite volume of molecules becomes important when cell sizes are reduced to the nanoscale. Therefore, a length scale that characterises the excluded volume of a molecule, d_{mol}, is introduced in mapping from an atomic model to a FHD representation. Each molecule is considered as a moving cube with a size of d_{mol}^3 and the density within is assumed to be uniform. Ignoring the finite size of molecules (the point-particle assumption) results in an overestimation of density fluctuations, whereas too large a value of d_{mol} would underestimate density fluctuations as a result of artificial spatial correlation. To justify that a d_{mol} value corresponding to the excluded volume of a molecule is adequate for describing the density fluctuations of a molecular liquid, it is used as an adjustable parameter to best fit the density fluctuations observed in all-atom MD and FHD simulations. The root of mean squared differences between the density fluctuations from MD and FHD simulations of argon (normalised by the averaged density) as a function of d_{mol} for four different decomposition cell sizes, d, are shown in Figure 3. It is clear that when large cell sizes are used for spatial discretisation, the overestimation of density fluctuations using the point-particle approximation becomes negligible. However, as the cell size approaches a few nanometres or less, density fluctuations become a much stronger function of d_{mol}, suggesting that an explicit consideration of the finite size of molecules is an important factor for bridging MD and FHD simulations of a fluid. Minimising the relative differences in density fluctuations between FH and MD by varying the effective molecular size results in a value of $d_{\mathrm{mol}} = 3.2$ Å for argon at 300 K. As shown in the inset of Figure 3, this value of d_{mol} also corresponds to the length scale of the excluded volume of argon as indicated by the radial distribution function, $g(r)$, computed from MD simulations. Analysis for liquid water also leads to a similar finding [18].

The results shown in Figure 3 demonstrate that an unbiased determination of d_{mol} can be made. Following this mapping, we compute the power spectrum, $C_t(q, \omega)$ (Fourier transform of momentum field auto-correlation function, $C_t(q, t)$) from all-atom MD simulation and compare the results with normal mode analysis of the

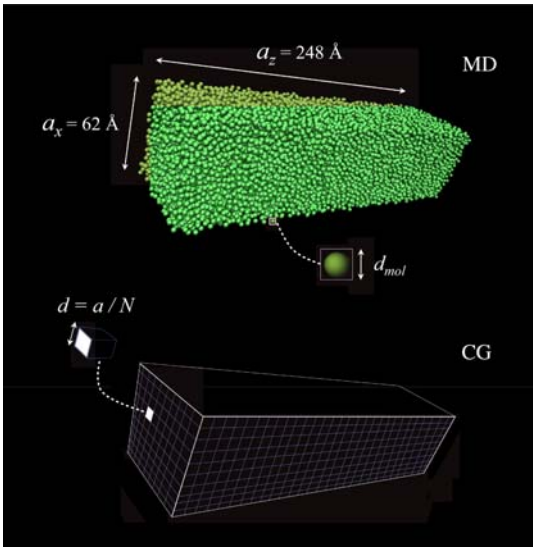

Figure 2. Atomistic (top) and CG (bottom) representations of a molecular fluid. The simulation box has side lengths a_β ($\beta = x, y, z$) and the length of each fluid cell d is calculated by $d = a_\beta/N_\beta$, where N_β is the number of cells used along each dimension for spatial discretisation. Each fluid molecule is assumed to have a volume of $(d_{\mathrm{mol}})^3$ and a uniform density field within. The contributions of each molecule to the density fields of overlapping cells can be easily calculated.

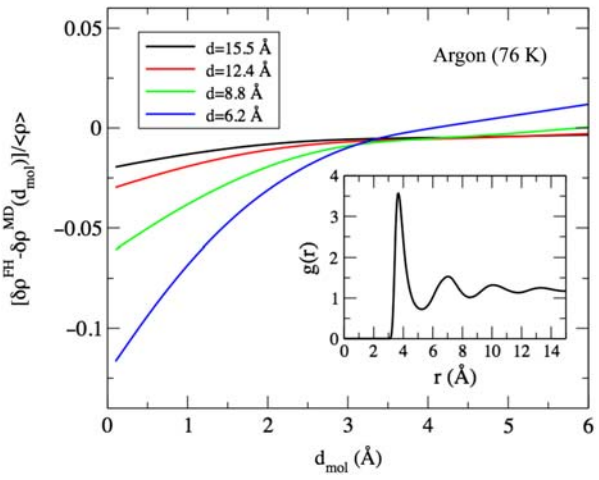

Figure 3. Differences in the normalised standard deviation of mass density $\delta\rho/\langle\rho\rangle$ between FHD and MD simulations as a function of d_{mol}. Results for five different cell sizes are shown. The inset corresponds to the centre-of-mass radial distribution function of argon calculated from all-atom MD simulation.

hydrodynamic equations using the composite viscoelastic model described earlier to characterise the emergent mechanical responses at the nanoscale and relevant transport parameters.

3. Results

In this section, we examine the emergent nanoscale viscoelasticity of fluids by bridging the FHD and MD simulations of a fluid. We first describe the details of all-atom MD simulations and the mapping procedure described in the previous section to develop a hydrodynamic model from the results of all-atom MD simulations. Through this mapping, we analyse the power spectra and examine whether the proposed Newtonian–Maxwell model can capture the wavenumber-dependent hydrodynamic fluctuations of molecular fluids. This approach is applied to characterise the transport properties of TIP3P water and argon at small length scales.

3.1 MD simulations of water and argon

Liquid water and argon are employed as illustrative examples for the methods developed in this work. We simulate liquid water using the TIP3P model [28] with 32,000 water molecules (96,000 atoms) in a periodic unit cell. The periodic boundary conditions are also used in the simulation of argon, which involves 20,325 atoms. A Lennard-Jones potential with a well depth of 0.238 kcal/mol and a van der Waals radius of 1.88 [29,30] is used to describe the inter-atomic interactions for liquid argon. A snapshot of MD simulation of argon is shown in the upper half of Figure 2. For both of the simulations of water and argon, a rectangular box of dimensions $62\,\text{Å} \times 62\,\text{Å} \times 248\,\text{Å}$ was used and the corresponding density is $0.6025\,\text{amu/Å}^3$ for water and $0.8489\,\text{amu/Å}^3$ for argon. This size of the simulation domain allows the analysis of hydrodynamic fluctuations over a broad range of wave vectors directly from the results of all-atom MD. The NAMD software is used for dynamic simulations [31]. Short-range non-bound interactions are smoothly switched off over a distance of 2 Å from 10 to 12 Å. A particle-mesh Ewald method is used to compute electrostatic interactions for the water simulation and the bond lengths of water are constrained at equilibrium values. After initial equilibration (at 300 K for water and 76 K or argon) via velocity scaling for 2 ps, MD simulations for both systems are conducted in the NVE ensemble with a 2 fs time step of integration. The water simulation is conducted for 20 ns and the argon simulation is conducted for 100 ns; no drifts in total energy or temperature are observed. A snapshot is saved every 0.2 ps to compute the power spectrum.

3.2 Wavenumber (q)-dependent viscoelasticity at the nanoscale

First, we perform a normal mode analysis on the linearised hydrodynamic equations of the composite Newtonian–Maxwell model described earlier to identify its hydrodynamic modes as a function of transport coefficients. In general, transport coefficients are wavenumber (q)-dependent [32]. For the composite Newtonian–Maxwell model (Equations (3)–(5)), the relevant transport coefficients include $v \equiv v_q$ (viscosity), $\mu \equiv \mu_q$ (elastic modulus) and $\tau \equiv \tau_q$ (time constant of memory effect). The resulting power spectrum is [24]:

$$C_t(q,\omega) = \frac{2q^2(\nu_q + \nu_q^{el}(\omega))}{[\omega - q^2(\omega\tau_q)\nu_q^{el}(\omega)]^2 + [q^2(\nu_q + \nu_q^{el}(\omega))]^2}. \tag{9}$$

In Equation (9), a kinematic viscosity that characterises the strength of elastic response is introduced:

$$\nu_q^{el}(\omega) = \frac{\mu_q\tau_q}{1+\omega^2\tau_q^2}. \tag{10}$$

Since the Maxwell model is added to the Newton's law in parallel, a total kinematic viscosity can be defined as:

$$\nu_q^{\text{tot}}(\omega) = \nu_q + \nu_q^{el}(\omega). \tag{11}$$

The values of ν_q and $\nu_q^{el}(0) = \mu_q\tau_q$ at zero frequency can be used to measure the relative magnitude of viscosity and elasticity by a dimensionless group, $\xi_q = \mu_q\tau_q/\nu_q$ [24].

To examine if the composite Newtonian–Maxwell model can be applied to capture the elastic responses that emerge at the nanoscale, we fit the power spectra calculated from MD simulations with the analytical form derived from normal mode analysis (Equation (9)). First, the zero-frequency component of the power spectrum, ν_q^{tot}, was obtained from MD simulation as an ensemble average, and ν_q was then determined from the values of ν_q^{tot} and ν_q^{el} from Equation (9). We then perform a least-squares fit by varying τ_q and ν_q^{el} to reproduce the computed profile from MD simulations. The large simulation domain of all-atom MD simulations we employed ($a_z = 248$ A) allowed the probe of hydrodynamic fluctuations over an unprecedented range of wavenumbers. The power spectra of argon and TIP3P calculated from MD simulations for three different wavenumbers are shown in Figure 4, along with the best-fit curve using Equation (9). Quantitative agreement between the simulated and analytical power spectra indicates that the composite Newtonian–Maxwell model captures the hydrodynamic fluctuations of water and argon, including the elasticity that emerges at high qs.

As q increases, elastic response leads to the characteristics of shear wave propagation instead of an exponential decay (e.g. Figure 4, $q = 0.304$ and $0.430\,\text{Å}^{-1}$

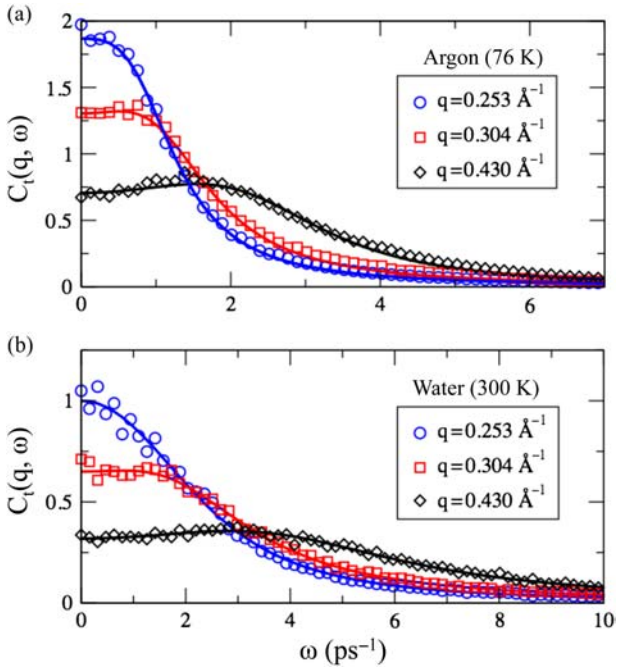

Figure 4. The power spectra of (a) argon and (b) TIP3P water calculated from atomistic MD simulations (open symbols) and the best-fit curves (solid lines) using Equation (9) for three different wavenumbers using q-dependent transport coefficients. Higher wavenumbers give rise to more pronounced elastic responses.

for both fluids). The calculated values of the dimensionless group ξ_q indicate that the elastic response is an increasing function of q for both argon and water [24]. ξ_q is almost zero at long wavelengths; as q increases, it quickly transits to the regime in which elastic responses are more pronounced than viscous responses [24]. For TIP3P water at 300 K, the Maxwell viscosity becomes significant compared with the Newtonian viscosity when the wavelength is reduced to 42 Å ($q = 0.15$ Å^{-1}). For argon at 76 K, the length scale for this transition is around 62.8 Å ($q = 0.1$ Å^{-1}) [24]. In addition to water and argon, the composite Newtonian–Maxwell model with q-dependent transport coefficients also accurately describes the power spectra of an $EMIM^+/NO_3^-$ ionic liquid obtained from all-atom MD simulations using a polarisable force field [24,33–35].

Comparison of Equation (9) with power spectra obtained from numerical FHD simulations with coloured noise demonstrates strong quantitative agreement between numerical results and the analytical formula across a broad range of wavenumbers [24]. Transport coefficients obtained from matching Equation (9) with the results of MD simulations can thus be readily employed in non-Markovian FHD simulations.

Despite the high accuracy of the composite Newtonian–Maxwell model in describing hydrodynamic fluctuations at the nanoscale, q-dependent transport coefficients complicates the application of this model in FHD simulations. Since the composite Newtonian–Maxwell model contains both viscous and elastic responses even with a single set of transport coefficients, an important question is whether a q-independent model can be used to approximate hydrodynamic fluctuations and the range of applicable wavelengths. In the following, we address this question by fitting the power spectra calculated from all-atom MD simulations using a q-independent model.

3.3 *Least-squares fit of power spectra using q-independent transport coefficients*

By using a single set of transport coefficients, we focus on important features of the power spectra (see Figure 4) for the fitting. In particular, the frequency of the peak location, ω^* and peak height, C_t^*, and the zero-frequency component, C_{t0} at different qs are employed as objective quantities. The overall strategy is to emphasise the accuracy of lower-frequency and longer-wavelength responses.

First, the values of $\omega^*(q)$, $C_t^*(q)$ and $C_{t0}(q)$ across all qs are determined from the power spectra using q-dependent transport parameters (the results of best fit to MD simulations). A least-squares fit was then performed by varying three parameters, τ, ν and μ, as follows. For each set $\{\nu, \mu, \tau\}$, the corresponding power spectra and hence $\omega^*(q)$, $C_t{*}(q)$ and $C_{t0}(q)$ for all wavenumbers are determined based on Equation (9). The difference of the values $\omega^*(q)$, $C_t{*}(q)$ and $C_{t0}(q)$ with target values is measured by:

$$R^2 = \sum_q \left\{ \begin{array}{l} [C_t^*(q;\{\nu,\mu,\tau\}) - C_t^{*(\mathrm{MD})}(q;\{\nu_q,\mu_q,\tau_q\})]^2 + \\ [\omega^*(q;\{\nu,\mu,\tau\}) - \omega^{*(\mathrm{MD})}(q;\{\nu_q,\mu_q,\tau_q\})]^2 + \\ [C_{t0}(q;\{\nu,\mu,\tau\}) - C_{t0}^{(\mathrm{MD})}(q;\{\nu_q,\mu_q,\tau_q\})]^2 \end{array} \right\}. \quad (12)$$

The values of ν, μ, τ are then adjusted to minimise R^2; the maximum q included in the fitting is 0.55 Å^{-1}.

The values of ν, μ and τ for argon and TIP3P water determined from this best-fit procedure are presented in Table 1. Since the composite Maxwell–Newtonian model splits the stress tensor into two parts, with the Maxwell part aiming to capture the elastic responses at the nanoscale, in the long-wavelength, zero-frequency limit, the total viscosity (Equation (11)) should correspond to the macroscopic viscosity of a molecular fluid. The values of the total zero-frequency kinematic viscosity v_{tot} (Equation (11)) determined by the best-fit procedure are 17.5 and 33.3 Å^2 ps^{-1} for argon and water, respectively. These results agree well with values of the macroscopic shear

Table 1. The q-independent transport properties of argon and TIP3P water determined by the least-squares fit procedure described in the text. The values of kinematic viscosity in the macroscopic regime determined by other simulation methods are also listed for comparison.

	Argon (76 K)	Water (300 K)
ν (Å^2 ps^{-1})	4.66	15.0
μ (Å^2 ps^{-2})	22.8	46.8
τ (ps)	0.562	0.390
ν_{el} (Å^2 ps^{-1})	12.8	18.3
ν_{tot} (Å^2 ps^{-1})	17.5	33.3
ν_0 (Å^2 ps^{-1})	19.9 [23]	34.8 [18]

viscosity, v_0, for argon at 76 K ($v_0 = 19.9$ Å^2 ps^{-1}) and water at 300 K ($v_0 = 34.8$ Å^2 ps^{-1}) obtained via other molecular simulations [18,23].

The power spectra using a single set of transport coefficients (q-independent) are compared with those using q-dependent transport coefficients in Figure 5. When $q < 0.25$ Å^{-1}, using q-independent transport coefficients captures the location and height of the peak in the power spectra due to elastic responses as well as the zero-frequency value with high accuracy. This result is seen in both argon and water (TIP3P). Therefore, using q-independent transport coefficients with the composite Newtonian–Maxwell model presents a good approximation for fluctuations with a wavelength longer than 25 Å. However, as the wavelength of fluctuations is reduced ($q > 0.25$ Å^{-1}), using a single set of transport coefficients results in a growing deviation from the power spectra computed from all-atom MD. Figure 6 shows the increasing relative error in $\omega^*(q)$, $C_t^*(q)$ and $C_{t0}(q)$ with q for both argon and water, when using a set of q-independent transport coefficients. The relative errors are determined based on the results calculated from MD simulations.

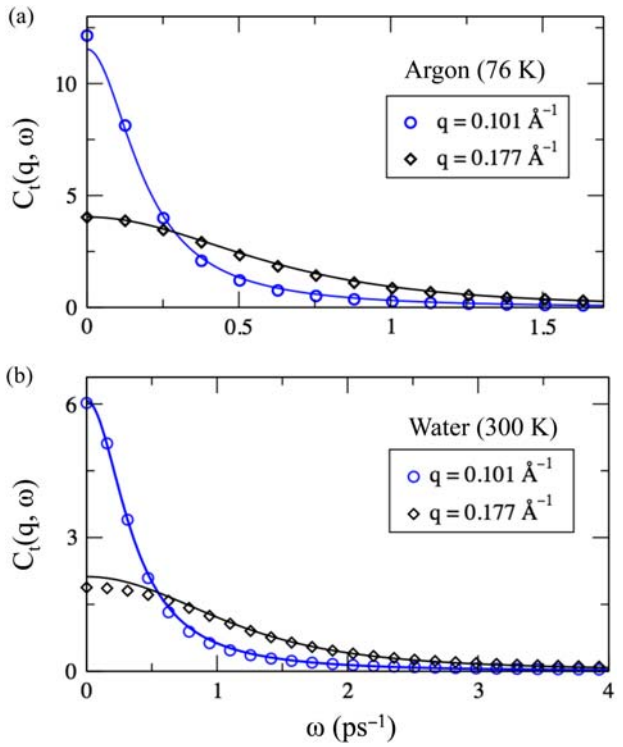

Figure 5. The power spectra of (a) argon and (b) TIP3P water from MD simulations calculated using a least-squares fit of Equation (9) for two wavenumbers. Open symbols represent results of using q-dependent transport coefficients (solid lines in Figure 4). Solid lines represent results using a single set of q-independent transport coefficients.

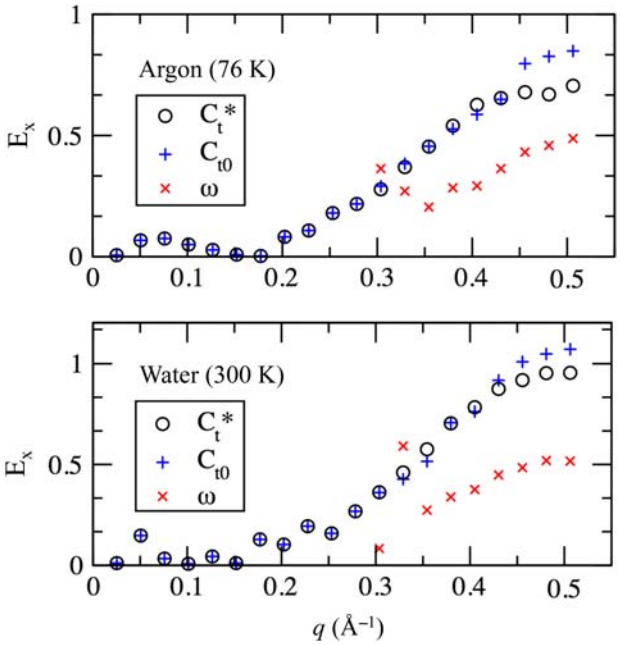

Figure 6. Relative error in $\omega^*(q)$, $C_t^*(q)$ and $C_{t0}(q)$ calculated as $E_x = |x' - x|/x$, where x is the resulting value obtained using q-dependent transport coefficients and x' is the value obtained using a single set of q-independent transport coefficients.

4. Conclusion

In this work, we outline a systematic methodology for modelling the rheological responses and thermal fluctuations of molecular fluids at the nanoscale. We show that the framework of FHD can be generalised to model the non-Markovian dynamics of field variables with coloured noise. To capture the emergent viscoelastic responses of molecular fluids at the nanoscale, we develop a composite Newtonian–Maxwell model. With careful consideration of the effective size of each molecule, we illustrate that the thermodynamic states and dynamic properties of FHD and atomic models can match each other quantitatively. To avoid the complexities associated with using q-dependent transport coefficients in FHD simulations,

we characterise the approximation using a single set of transport coefficients in the composite Maxwell–Newtonian model. We found that for both liquid water and argon, q-independent models can accurately describe the collective fluctuations with a wavelength longer than 25 Å. For fluctuations with shorter wavelengths, relative errors in power spectra increase monotonically with wavenumber.

Acknowledgements

We thank Berni Alder and Aleksandar Donev for insightful discussions. This research is supported by Grant No. ACS-PRF-49727-DNI6 and by the College of Chemistry at University of California, Berkeley.

References

[1] R.K. Soong, G.D. Bachand, H.P. Neves, A.G. Olkhovetes, H.G. Craighead, and C.D. Montemagno, *Powering an inorganic nanodevice with a biomolecular motor*, Science 290 (2000), pp. 1555–1558.

[2] M. Moseler and U. Landman, *Formation, stability and breakup of nanojets*, Science 289 (2000), pp. 1165–1169.

[3] K. Kadau, T.C. Germann, N.G. Hadjiconstantinou, et al., *Nanohydrodynamics simulations: An atomistic view of the Rayleigh-Taylor instability*, Proc. Natl Acad. Sci. USA 101 (2004), pp. 5851–5855.

[4] E. Meyer, T. Gyalog, and R.M. Overney, *Nanoscience: Friction and Rheology on the Nanometer Scale*, World Scientific, Singapore, 2002.

[5] J.C.T. Eijkel and A.v.d. Berg, *Nanofluidics: what is it and what can we expect from it*?, Microfluid. Nanofluid. 1 (2005), pp. 249–267.

[6] J. Howard, *Mechanics of Motor Proteins and the Cytoskeleton*, Sinauer Associates, Sunderland, MA, 2001.

[7] S.J. Bussell, D.L. Koch, and D.A. Hammer, *Effect of hydrodynamic interactions on the diffusion of integral membrane proteins: tracer diffusion in organelle and reconstruction membranes*, Biophys. J. 68 (1995), pp. 1828–1835.

[8] L.D. Landau and E.M. Lifshitz, *Fluid Mechanics*, Pergamon, New York, 1959.

[9] J.J. Monaghan, *Smoothed particle hydrodynamics*, Annu. Rev. Astron. Astrophys. 30 (1992), pp. 543–574.

[10] A.J.C. Ladd, *Short-time motion of colloidal particles: Numerical simulation via fluctuating lattice-Boltzmann equation*, Phys. Rev. Lett. 70 (1993), pp. 1339–1342.

[11] P.J. Hoogerbrugge and J.M.V.A. Koelman, *Simulating microscopic hydrodynamic phenomena with dissipative particle dynamics*, Europhys. Lett. 19 (1992), pp. 155–160.

[12] P. Espanol, *Dissipative particle dynamics with energy conservation*, Europhys. Lett. 40 (1997), pp. 631–636.

[13] P.R. Kramer , C.S. Peskin, and K.J. Bathe, *Computational Fluid and Solid Mechanics 2003*, Elsevier Science Ltd., Oxford, 2003, p. 1755.

[14] P.J. Atzberger, P.R. Kramer, and C.S. Peskin, *A stochastic immersed boundary method for fluid-structure dynamics at microscopic length scales*, J. Comput. Phys. 224 (2007), pp. 1255–1292.

[15] J.B. Bell, A.L. Garcia, and S.A. Williams, *Numerical methods for the stochastic Landau–Lifshitz: Navier-Stokes equations*, Phys. Rev. E (Stat. Nonlin. Soft Matter Phys.) 76 (2007), pp. 016708-1–016708-12.

[16] P. Espanol, *Stochastic differential equations for non-linear hydrodynamics*, Physica A 248 (1998), pp. 77–96.

[17] G. De Fabritiis, M. Serrano, R. Delgado-Buscalioni, and P.V. Coveney, *Fluctuating hydrodynamic modeling of fluids at the nanoscale*, Phys. Rev. E (Stat. Nonlin. Soft Matter Phys.) 75 (2007), pp. 026307-1–026307-11.

[18] N.K. Voulgarakis and J.-W. Chu, *Bridging fluctuating hydrodynamics and molecular dynamics simulations of fluids*, J. Chem. Phys. 130 (2009), pp. 134111-1–134111-9.

[19] J.H. Irving and J. Kirkwood, *The statistical mechanical theory of transport processes. IV. The equations of hydrodynamics*, J. Chem. Phys. 18 (1950), pp. 817-1–817-13.

[20] B.D. Todd, J.S. Hansen, and P.J. Daivis, *Nonlocal shear stress for homogeneous fluids*, Phys. Rev. Lett. 100 (2008), pp. 195901-1–195901-4.

[21] R. Zwanzig and R. Mountain, *High-frequency elastic moduli of simple fluids*, J. Chem. Phys. 43 (1965), pp. 4464–4471.

[22] R. Zwanzig and R. Mountain, *Shear relaxation times of simple fluids*, J. Chem. Phys. 44 (1966), pp. 2771–2779.

[23] R. Zwanzig and M. Bixon, *Hydrodynamic theory of the velocity correlation function*, Phys. Rev. A 2 (1970), pp. 2005–2012.

[24] N.K. Voulgarakis, S. Satish, and J.-W. Chu, *Modeling the nanoscale viscoelasticity of fluids by bridging non-Markovian fluctuating hydrodynamics and molecular dynamic simulations*, J. Chem. Phys. 131 (2009), pp. 234115-1–234115-8.

[25] I. Ispolatov and M. Grant, *Lattice Boltzmann method for viscoelastic fluids*, Phys. Rev. E 65 (2002), pp. 056704-1–056704-4.

[26] R. Zwanzig, *Nonlinear generalized Langevin equations*, J. Stat. Phys. 9 (1973), pp. 215–220.

[27] C.-H. Chung and S. Yip, *Generalized hydrodynamics and time correlation functions*, Phys. Rev. 182 (1969), pp. 323–339.

[28] N.K. Ailawadi, A. Rahman, and R. Zwanzig, *Generalized hydrodynamics and analysis of current correlation function*, Phys. Rev. A 4 (1971), pp. 1616–1625.

[29] A. Bondi, *van der Waals volumes and radii*, J. Phys. Chem. 68 (2002), pp. 441–451.

[30] L. Verlet, *Computer "experiments" on classical fluids. I. Thermodynamical properties of Lennard-Jones molecules*, Phys. Rev. 159 (1967), pp. 98–103.

[31] L. Kalè, R. Skeel, M. Bhandarkar, R. Brunner, A. Gursoy, N. Krawetz, J. Phillips, A. Shinozaki, K. Varadarajan, and K. Schulten, *NAMD2: greater scalability for parallel molecular dynamics*, J. Comput. Phys. 151 (1999), pp. 283–312.

[32] J.P. Boon and S. Yip, *Molecular Hydrodynamics*, Courier Dover Publications, North Chelmsford, MA, 1991.

[33] M.G. Del Popolo and G.A. Voth, *On the structure and dynamics of ionic liquids*, J. Phys. Chem. B 108 (2004), pp. 1744–1752.

[34] T. Yan, C.J. Burnham, M.G. Del Pópolo, and G.A. Voth, *Molecular dynamics simulation of ionic liquids: The effect of electronic polarizability*, J. Phys. Chem. B 108 (2004), pp. 11877–11881.

[35] Y. Wang, S. Izvekov, T. Yan, and G.A. Voth, *Multiscale coarse-graining of ionic liquids*, J. Phys. Chem. B 110 (2006), pp. 3564–3575.